Journal of Computational Physics **161,** 70–84 (2000)
doi:10.1006/jcph.2000.6487, available online at http://www.idealibrary.com on IDEAL®

Simulations of Compressible Flows with Strong Shocks by an Adaptive Lattice Boltzmann Model

Chenghai Sun

Department of Engineering Mechanics, State Key Laboratory of Tribology, Tsinghua University, Beijing, 100084, People's Republic of China
E-mail: sunch@mail.tsinghua.edu.cn

Received September 30, 1998; revised February 21, 2000

An adaptive lattice Boltzmann model for compressible flows is presented. The particle-velocity set is so large that the mean flow may have a high velocity. The support set of the equilibrium-distribution function is quite small and varies with the mean velocity and internal energy. The adaptive nature of this support set permits the mean flows to have high Mach number, meanwhile, it makes the model simple and practicable. The model is suitable for perfect gases with an arbitrary specific heat ratio. Navier–Stokes equations are derived by the Chapman–Enskog method from the BGK Boltzmann equation. When the viscous terms and the diffusion terms are considered as a discretion error this system becomes an inviscid Euler system. Several simulations of flows with strong shocks, including the forward-facing step test, double Mach reflection test, and a strong shock of Mach number 5.09 diffracting around a corner, were carried out on hexagonal lattices, showing the model's capability of simulating the propagation of strong shock waves.

Key Words: lattice Boltzmann; Euler equation; N-S equation; adaptive velocities; perfect gas.

I. INTRODUCTION

In the past years, the lattice Boltzmann (LB) method has attracted much attention as a novel alternative to traditional methods for numerically solving the Navier–Stokes (N-S) equation. The LB method has demonstrated its ability to simulate single component hydrodynamics, multiphase and multi-component fluids, magneto-hydrodynamics, reaction-diffusion systems, flows through porous media, and other complex systems (see a review paper [1]). Meanwhile, the LB method has demonstrated a significant potential and broad applicability with numerous computational advantages, such as the parallel of algorithm, the simplicity of programming, and the ability to incorporate microscopic interactions. Although promising, the current lattice Boltzmann method still has a few

0021-9991/00 $35.00

undesirable shortcomings that limit its general application as a practical computational fluid dynamics tool. One of these shortcomings, which is specifically addressed in this paper, is the low Mach number constraint.

Historically, the LB method originated from a Boolean model known as *l*attice *g*as *a*utomata (LGA) [2, 3]. The standard LGA models impose, for the sake of computational efficiency, a Boolean constraint which restricts the number of particles with a given velocity at a site to be zero or one. The local equilibrium of the mean population of particles is described by the Fermi–Dirac statistics. As a result, LGA models suffer from the statistical noise and the non-Galilean invariance. These difficulties have led to the development of LB models [4–6]. In LB method real numbers represent the local ensemble-averaged particle distribution functions. The simple Bhatnagar–Gross–Krook (BGK) collision operator is applied [4, 5]. Space and time are discrete as they are in the LGA method. The particle velocities belong to a finite set. Consequently the macroscopic velocity is limited. As a result, the general LB method suffers from the constraint of small Mach number. The gas-kinetic theory [7, 8] and the discrete-velocity model [9] successfully simulated the compressible Euler equation. The finite volume method was employed to solve the Boltzmann equations. The discontinuities were well captured. However, due to the restraint mentioned above, the standard LB method has great difficulty to simulate compressible Euler flows at high Mach number. Many efforts have been made to overcome this difficulty in the past years. Alexander *et al.* [10] attempted to decrease the sound speed to augment the Mach number. Hu *et al.* [11] proposed a compressible LB model for Euler system and simulated the Sod shock-tube problem. Recently, we proposed a locally adaptive LB model [12]. The particle velocity set is chosen so large that the fluid velocity is no longer limited by it. Consequently, the model is suitable for a wide range of Mach number. We have successfully simulated the Sod shock-tube problem and two-dimensional shock reflection. This model has been extended to a thermal adaptive LB model [13, 14].

In the present paper, we formulate a generalized adaptive LB model in which both the particle velocity phase and the particle energy phase are continuous spaces. Then we simulate several standard flow problems to demonstrate the capability of this model for capturing strong shock waves. This paper is organized as follow. The first part of Section II describes the generalized adaptive LB model and derives the general macroscopic conservation equations from the Boltzmann equations by the Chapman–Enskog method. In the second part an equilibrium distribution function is determined such that the general macroscopic conservation equations become the N-S equations. The third part discusses the stability of the model. Section III is about the numerical results. Finally, some concluding remarks will be presented.

II. SEMI-DISCRETE ADAPTIVE LB MODEL

A. *Basic equations.* Let $\mathbf{r}$ be the particle "migrating velocity," transporting a particle from a node to its neighbor node at a distance $\mathbf{r}\Delta t$ during the discrete time Δt. Let S be a set of migrating velocities, $S = \{\mathbf{r}\}$. Because the nodes of the lattice are discrete this set is discrete. Suppose that the particle transports the mass m, momentum $m\boldsymbol{\xi}$, and energy $m\zeta$ to the neighbor node at a distance $\mathbf{r}\Delta t$, where $\boldsymbol{\xi}$ and ζ are called particle "phase velocity" and "phase energy," and m is the particle mass. $\boldsymbol{\xi} \in \mathcal{D}_1$, $\mathcal{D}_1$ is a bounded domain in $\Re^3$ (or in $\Re^2$ for 2-D models) and $\mathbf{r} \in \mathcal{D}_1$; $\zeta \in \mathcal{D}_0$, $\mathcal{D}_0$ is a bounded domain in $\Re$. Define $\mathcal{D} = \mathcal{D}_1 \times \mathcal{D}_0$. In other words, the migrating velocity $\mathbf{r}$ is used to calculate the distance that the particle moves;

the phase velocity $\boldsymbol{\xi}$ and phase energy ζ are used to calculate the momentum and energy transported by the particle. Unlike the migrating velocity $\mathbf{r}$ which is discrete, $\boldsymbol{\xi}$ and ζ can vary continuously. Therefore we call this model a "semi-discrete model." In the standard LB model, space, time, and the particle velocity are all discrete; as a result, $\boldsymbol{\xi}$ and ζ must be discrete and take the values of $\mathbf{r}$ and $\frac{1}{2}\mathbf{r}^2$, respectively. The objective of introducing such a semi-discrete velocity LB model is to increase accuracy of the model [12].

Let $\mathbf{x}$ be an arbitrary node of a lattice; $f(\mathbf{x}, \mathbf{r}, \boldsymbol{\xi}, \zeta, t)$ is the density distribution function for the particle with the phase velocity $\boldsymbol{\xi}$ and migrating velocity $\mathbf{r}$, moving to $\mathbf{x}+\mathbf{r}\Delta t$ during Δt, and transporting the momentum $m\boldsymbol{\xi}$ and energy $m\zeta$. The conserved total mass, momentum, and energy are defined as

$$\rho \equiv \sum_{\mathbf{r}\in S} \int_{\mathcal{D}} m f(\mathbf{x}, \mathbf{r}, \boldsymbol{\xi}, \zeta, t)\, d\boldsymbol{\xi}\, d\zeta \tag{1}$$

$$\rho\mathbf{v} \equiv \sum_{\mathbf{r}\in S} \int_{\mathcal{D}} m\boldsymbol{\xi} f(\mathbf{x}, \mathbf{r}, \boldsymbol{\xi}, \zeta, t)\, d\boldsymbol{\xi}\, d\zeta \tag{2}$$

$$\rho E \equiv \sum_{\mathbf{r}\in S} \int_{\mathcal{D}} m\zeta f(\mathbf{x}, \mathbf{r}, \boldsymbol{\xi}, \zeta, t)\, d\boldsymbol{\xi}\, d\zeta, \tag{3}$$

where $d\boldsymbol{\xi} = d\xi_1\, d\xi_2\, d\xi_3$.

It is pointed out that the vectors in S need not to be different one from each other; they are, however, considered as different elements and the sum is taken over all the elements in S. Define

$$\boldsymbol{\eta} \equiv [m, m\boldsymbol{\xi}, m\zeta]^{\mathrm{T}} \tag{4}$$

$$\mathbf{Y} \equiv [\rho, \rho\mathbf{v}, \rho E]^{\mathrm{T}}. \tag{5}$$

The formulae (1), (2), (3) can be written in the compact form,

$$\mathbf{Y} = \sum_{\mathbf{r}\in S} \int_{\mathcal{D}} \boldsymbol{\eta} f(\mathbf{x}, \mathbf{r}, \boldsymbol{\xi}, \zeta, t)\, d\boldsymbol{\xi}\, d\zeta. \tag{6}$$

In LB models, the distribution function $f(\mathbf{x}, \mathbf{r}, \boldsymbol{\xi}, \zeta, t)$ satisfies the BGK Boltzmann equation,

$$\begin{gathered} f(\mathbf{x}+\mathbf{r}\Delta t, \mathbf{r}, \boldsymbol{\xi}, \zeta, t+\Delta t) - f(\mathbf{x}, \mathbf{r}, \boldsymbol{\xi}, \zeta, t) = \Omega(\mathbf{x}, \mathbf{r}, \boldsymbol{\xi}, \zeta, t) \\ \mathbf{r} \in S, \qquad \boldsymbol{\xi} \in \mathcal{D}_1, \qquad \zeta \in \mathcal{D}_0, \end{gathered} \tag{7}$$

where

$$\Omega(\mathbf{x}, \mathbf{r}, \boldsymbol{\xi}, \zeta, t) = -\frac{1}{\tau}[f(\mathbf{x}, \mathbf{r}, \boldsymbol{\xi}, \zeta, t) - f^{\mathrm{eq}}(\mathbf{x}, \mathbf{r}, \boldsymbol{\xi}, \zeta, t)] \tag{8}$$

and $f^{\mathrm{eq}}(\mathbf{x}, \mathbf{r}, \boldsymbol{\xi}, \zeta, t)$ is the equilibrium distribution depending on the total mass, momentum, and energy. The discrete migrating velocity set $\{\mathbf{r}\}$ is large; moreover, $\boldsymbol{\xi}$ and ζ can

vary continuously. Therefore, the Boltzmann Eq. (7), in general, is hard to solve. In fact, Eq. (7) is only used for theoretical analysis. The technique for numerical simulation will be discussed in Section III.

In the following, we utilize the Chapman–Enskog expansion of the solution of Eq. (7) to derive the macroscopic conservation equations [16–18]. We choose $\Delta t = \epsilon T$, where T is a reference time scale and ϵ a typical small parameter. We are then looking for a solution of Eq. (7) as an asymptotic expansion of the form

$$f = \sum_{n=0}^{\infty} \epsilon^n f^{(n)} \tag{9}$$

$$\frac{\partial \mathbf{Y}}{\partial t} = \sum_{n=0}^{\infty} \epsilon^n \mathbf{F}^{(n)}, \tag{10}$$

where $f^{(n)}$ and $\mathbf{F}^{(n)}$ depend only on $\mathbf{Y}$ and its successive gradients. $f^{(0)} = f^{\mathrm{eq}}$ is completely determined by the macroscopic variables ρ, $\rho\mathbf{v}$, and ρE and satisfies

$$\mathbf{Y} = \sum_{\mathbf{r}\in S} \int_{\mathcal{D}} \boldsymbol{\eta} f^{\mathrm{eq}}(\mathbf{x}, \mathbf{r}, \boldsymbol{\xi}, \zeta, t)\, d\boldsymbol{\xi}\, d\zeta. \tag{11}$$

Considering the relations (6), (11), (9), and (8) we have

$$\sum_{\mathbf{r}\in S} \int_{\mathcal{D}} \boldsymbol{\eta} f^{(n)}\, d\boldsymbol{\xi}\, d\zeta = 0, \qquad \forall n \geq 1 \tag{12}$$

$$\sum_{\mathbf{r}\in S} \int_{\mathcal{D}} \boldsymbol{\eta}\Omega\, d\boldsymbol{\xi}\, d\zeta = 0. \tag{13}$$

$\boldsymbol{\eta}$ is called "collision invariant."

We Taylor expand the left-hand side of Eq. (7). Then, by identifying the first-order terms of ϵ, we can determine $f^{(1)}$, and considering (12) and (13), we obtain $\mathbf{F}^{(0)}$ and $\mathbf{F}^{(1)}$,

$$f^{(1)} = -\tau T \left\{ \nabla f^{\mathrm{eq}} \cdot \mathbf{r} + \frac{\partial f^{\mathrm{eq}}}{\partial \mathbf{Y}} \cdot \mathbf{F}^{(0)} \right\}$$

$$\mathbf{F}^{(0)} = -\mathrm{div} \sum_{\mathbf{r}\in S} \int_{\mathcal{D}} \mathbf{r} f^{\mathrm{eq}} \boldsymbol{\eta}\, d\boldsymbol{\xi}\, d\zeta$$

$$\mathbf{F}^{(1)} = -\mathrm{div} \sum_{\mathbf{r}\in S} \int_{\mathcal{D}} \left\{ f^{(1)}\mathbf{r} + \frac{T}{2} \left[\mathrm{div}(f^{\mathrm{eq}}\mathbf{r}\mathbf{r}) + \frac{\partial f^{\mathrm{eq}}}{\partial \mathbf{Y}} \cdot \mathbf{F}^{(0)}\mathbf{r} \right] \right\} \boldsymbol{\eta}\, d\boldsymbol{\xi}\, d\zeta.$$

The operator div and ∇ take effect on variable $\mathbf{x}$. The variables $\mathbf{r}$, $\boldsymbol{\xi}$, and ζ are independent of $\mathbf{x}$. Therefore, they can be treated as constant for div and ∇. Up to order 1, Eq. (10) is written as

$$\frac{\partial \mathbf{Y}}{\partial t} = -\mathrm{div} \sum_{\mathbf{r}\in S} \int_{\mathcal{D}} f^{\mathrm{eq}} \mathbf{r} \boldsymbol{\eta}\, d\boldsymbol{\xi}\, d\zeta$$
$$-\epsilon T \left(\frac{1}{2} - \tau \right) \mathrm{div} \left[\mathrm{div} \sum_{\mathbf{r}\in S} \int_{\mathcal{D}} f^{\mathrm{eq}} \mathbf{r}\mathbf{r} \boldsymbol{\eta}\, d\boldsymbol{\xi}\, d\zeta + \sum_{\mathbf{r}\in S} \int_{\mathcal{D}} \frac{\partial f^{\mathrm{eq}}}{\partial \mathbf{Y}} \cdot \mathbf{F}^{(0)} \mathbf{r} \boldsymbol{\eta}\, d\boldsymbol{\xi}\, d\zeta \right]. \tag{14}$$

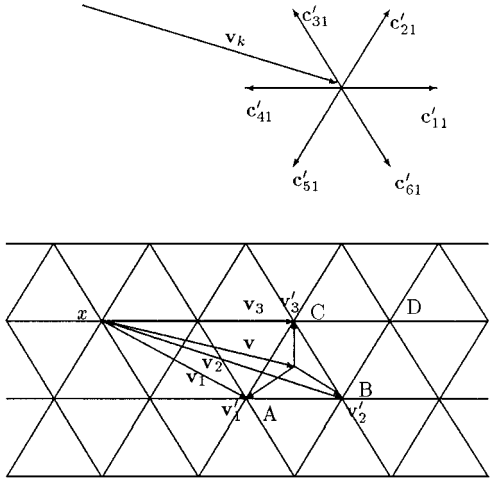

FIG. 1. Illustration of particle migrating velocities (for $\Delta t = 1$).

This is the macroscopic conservation equation. It depends on the distribution of f^{eq}. If the equilibrium distribution is properly determined it may become the N-S equations.

B. *Equilibrium distributions.* Let l be the unit length of a uniform lattice. Let's consider a vector set $\{\mathbf{c}'_{j\nu};\ j = 1, \ldots, b_\nu\}$ connecting a node to its equal distance neighbor nodes, where b_ν is the number of vector directions. c'_ν, the module of $\mathbf{c}'_{j\nu}$, is an integer times $l/\Delta t$. Suppose the vector set $\{\mathbf{c}'_{j\nu};\ j = 1, \ldots, b_\nu\}$ is symmetric up to order 2; i.e, $\sum_{j=1}^{b_\nu} \mathbf{c}'_{j\nu} = \mathbf{0}$ and $\sum_{j=1}^{b_\nu} \mathbf{c}'_{j\nu}\mathbf{c}'_{j\nu} = (c'^2_\nu/D)\mathbf{I}$, where $\mathbf{I}$ is second order unit tensor and D is the dimension of space [3]. For the hexagonal lattice we choose $b_\nu = 6$, $\nu = 1$ and 2. In the standard LB method, the constant vectors $\mathbf{c}'_{j\nu}$ are the particle velocities. We superimpose the fluid velocity $\mathbf{v}$, which is approximated by $\mathbf{v}_k$ ($k = 1, 2, 3$) (see Fig. 1), on the symmetric velocity $\mathbf{c}'_{j\nu}$. Let $\mathbf{x}$ be an arbitrary node; $\mathbf{v}$ is the fluid velocity at this node; $\mathbf{v}_1$, $\mathbf{v}_2$, and $\mathbf{v}_3$ are the vectors from the node $\mathbf{x}$ to the apexes of the triangle containing the velocity vector $\mathbf{v}$. Consider particle migrating velocities $\mathbf{c}_{j\nu k} \in S$, phase velocities $\bar{\mathbf{c}}_{j\nu} \in \mathcal{D}_1$, fluctuating velocities $\mathbf{v}'_k$ ($k = 1$, 2, 3), and phase energy $\zeta_{j\nu} \in \mathcal{D}_0$ defined by

$$\mathbf{c}_{j\nu k} = \mathbf{v}_k + \mathbf{c}'_{j\nu} \tag{15}$$

$$\bar{\mathbf{c}}_{j\nu} = \mathbf{v} + \mathbf{c}'_{j\nu} \tag{16}$$

$$\mathbf{v}_k = \mathbf{v} + \mathbf{v}'_k \tag{17}$$

$$\zeta_{j\nu} = \frac{1}{2}\bar{\mathbf{c}}^2_{j\nu} + \Phi = \frac{1}{2}\left(v^2 + 2\mathbf{c}_{j\nu}\cdot\mathbf{v} + c'^2_\nu\right) + \Phi. \tag{18}$$

$\zeta_{j\nu}$ consists of kinetic energy $m\frac{1}{2}\bar{\mathbf{c}}^2_{j\nu}$ and other form energy $m\Phi$ that was introduced in order to obtain an arbitrary specific heat ratio γ. Figure 1 shows the particle migrating velocities for $\Delta t = 1$. If Δt is not equal to 1, all the velocities in this figure should be multiplied by Δt. For high speed flow the fluctuating velocities $\mathbf{v}'_k$ are small.

We are now determining the equilibrium distribution $f^{\mathrm{eq}}(\mathbf{x}, \mathbf{r}, \boldsymbol{\xi}, \zeta, t)$, $\mathbf{r} \in S$, $\boldsymbol{\xi} \in \mathcal{D}_1$, $\zeta \in \mathcal{D}_0$. Suppose that the migrating velocity set S contains all $\mathbf{c}_{j\nu k}$ and that $\mathcal{D}$ ($=\mathcal{D}_1 \times \mathcal{D}_0$) is so large that $\bar{\mathbf{c}}_{j\nu} \in \mathcal{D}_1$ and $\zeta_{j\nu} \in \mathcal{D}_0$ for all $\bar{\mathbf{c}}_{j\nu}$ and $\zeta_{j\nu}$ all the time. We hope the model is as simple as possible under the condition that the fluid properties can be completely satisfied. We concentrate the particles at $\mathbf{r} = \mathbf{c}_{j\nu k}$, $\boldsymbol{\xi} = \bar{\mathbf{c}}_{j\nu}$, and $\zeta = \zeta_{j\nu}$.

We define the equilibrium distribution as

$$f^{\mathrm{eq}}(\mathbf{x},\mathbf{r},\boldsymbol{\xi},\zeta,t)\equiv\begin{cases} d_{\nu k}\delta(\boldsymbol{\xi}-\bar{\mathbf{c}}_{j\nu})\delta(\zeta-\zeta_{j\nu}) & \text{for } \mathbf{r}=\mathbf{c}_{j\nu k}\\ 0 & \text{for other } \mathbf{r}\in S,\end{cases} \tag{19}$$

where $\delta(\boldsymbol{\xi})$ is the δ function. $\delta(\boldsymbol{\xi})=0$ for $\boldsymbol{\xi}\neq 0$; $\int g(\boldsymbol{\xi})\delta(\boldsymbol{\xi})\,d\boldsymbol{\xi}=g(\mathbf{0})$. $\delta(\zeta)=0$ for $\zeta\neq 0$; $\int g(\zeta)\,\delta(\zeta)\,d\zeta=g(0)$. $d_{\nu k}$ is a function of macroscopic variables and will be determined later.

It is pointed out that $f^{\mathrm{eq}}(\mathbf{x},\mathbf{r},\boldsymbol{\xi},\zeta,t)$ is defined for all $(\mathbf{r},\boldsymbol{\xi},\zeta)\in S\times\mathcal{D}_1\times\mathcal{D}_0$. However, $f^{\mathrm{eq}}(\mathbf{x},\mathbf{r},\boldsymbol{\xi},\zeta,t)$ is non-zero only for $(\mathbf{r},\boldsymbol{\xi},\zeta)\in\{\mathbf{c}_{j\nu k}\}\times\{\bar{\mathbf{c}}_{j\nu}\}\times\{\zeta_{j\nu}\}$ that is called the support set of $f^{\mathrm{eq}}(\mathbf{x},\mathbf{r},\boldsymbol{\xi},\zeta,t)$. Define

$$f^{\mathrm{eq}}_{j\nu k}(\mathbf{x},t)\equiv\int_{\mathcal{D}} f^{\mathrm{eq}}(\mathbf{x},\mathbf{c}_{j\nu k},\boldsymbol{\xi},\zeta,t)\,d\boldsymbol{\xi}\,d\zeta=d_{\nu k}. \tag{20}$$

Substituting f^{eq} defined by Eq. (19) into Eq. (14), one obtains

$$\begin{aligned}\frac{\partial\mathbf{Y}}{\partial t}=-\mathrm{div}\sum_{k,\nu,j}\Bigg\{&d_{\nu k}\mathbf{c}_{j\nu k}\boldsymbol{\eta}'_{j\nu}+\epsilon T\left(\frac{1}{2}-\tau\right)\Bigg[\mathrm{div}(d_{\nu k}\mathbf{c}_{j\nu k}\mathbf{c}_{j\nu k}\boldsymbol{\eta}'_{j\nu})\\&+\mathbf{F}^{(0)}\cdot\frac{\partial}{\partial\mathbf{Y}}(d_{\nu k}\mathbf{c}_{j\nu k}\boldsymbol{\eta}'_{j\nu})\Bigg]\Bigg\},\end{aligned} \tag{21}$$

where

$$\boldsymbol{\eta}'_{j\nu}=\{m,m\bar{\mathbf{c}}_{j\nu},m\zeta_{j\nu}\}^{\mathrm{T}}=\left\{m,m(\mathbf{v}+\mathbf{c}'_{j\nu}),m\left[\frac{1}{2}(\mathbf{v}+\mathbf{c}'_{j\nu})^2+\Phi\right]\right\}^{\mathrm{T}}. \tag{22}$$

In the same way, Eq. (11) becomes

$$\mathbf{Y}=\sum_{\mathbf{r}\in S}\int_{\mathcal{D}}\boldsymbol{\eta}\,f^{\mathrm{eq}}(\mathbf{x},\mathbf{r},\boldsymbol{\xi},\zeta,t)\,d\boldsymbol{\xi}\,d\zeta=\sum_{k,\nu,j}d_{\nu k}\boldsymbol{\eta}'_{j\nu}, \tag{23}$$

i.e.,

$$\rho=\sum_{k,\nu}mb_\nu d_{\nu k}=\sum_{k=1}^{3}\rho_k \tag{24}$$

$$\begin{aligned}\rho E&=\sum_{k,\nu,j}md_{\nu k}\left(\frac{1}{2}\bar{c}^2_{j\nu}+\Phi\right)\\&=\sum_{k,\nu,j}\frac{1}{2}md_{\nu k}\left(\mathbf{v}^2+2\mathbf{v}\cdot\mathbf{c}'_{j\nu}+c'^2_\nu\right)+\rho\Phi\\&=\frac{1}{2}\rho\mathbf{v}^2+\sum_{k,\nu}\frac{1}{2}mb_\nu d_{\nu k}c'^2_\nu+\rho\Phi,\end{aligned} \tag{25}$$

where $\rho_k=\sum_\nu mb_\nu d_{\nu k}$. The second component of (23) is automatically satisfied as long as the $d_{\nu k}$ satisfy (24).

In order to increase the accuracy we assume that the ρ_k satisfy the equation

$$\rho\mathbf{v}=\sum_{k=1}^{3}\rho_k\mathbf{v}_k. \tag{26}$$

For given ρ and $\rho\mathbf{v}$ it can be proved that Eqs. (24) and (26) have unique non-negative solution for ρ_k (see Fig. 1). In fact, when the head of vector $\mathbf{v}$ is inside of the triangle ABC, ρ_k is positive for $k = 1, 2, 3$. When it approaches the segment BC, ρ_1 tends to 0. When it moves still further into the triangle BCD, the triangle ABC in consideration is replaced by BCD, and ρ_1, that is for point D now, becomes again positive. In brief, the ρ_k's change continuously when the head of vector $\mathbf{v}$ moves from a triangle into another one. If the head of vector $\mathbf{v}$ is on A we have $\rho_1 = \rho$, $\rho_2 = \rho_3 = 0$.

Equations (24) and (26) permit us to write

$$\sum_k \rho_k \mathbf{v}'_k = \mathbf{0}. \tag{27}$$

Thanks to Eq. (27), we will see that the first order of $\mathbf{v}'_k$ in the conservation equations will disappear. We introduce the density portion $\alpha_k = \rho_k/\rho$ and suppose $d_{\nu k}$ has the form

$$d_{\nu k} = \alpha_k d_\nu, \tag{28}$$

where $d_\nu = \sum_k d_{\nu k}$ will be determined by the density and pressure (or internal energy).

The perfect gas with specific heat ratio γ satisfies $p = (\gamma - 1)\rho e$, where $e = E - \frac{1}{2}v^2$ is the internal energy. The pressure p has the form

$$p = \sum_\nu m b_\nu d_\nu \frac{1}{D} c'^2_\nu, \tag{29}$$

where D is the space dimension.

In the case where the c'_ν have two levels ($\nu = 1, 2$) one can determine d_1, d_2, and Φ by Eqs. (24), (25), and (29),

$$d_1 = \rho \frac{c'^2_2 - D(\gamma - 1)e}{b_1 m\left(c'^2_2 - c'^2_1\right)}$$

$$d_2 = \rho \frac{D(\gamma - 1)e - c'^2_1}{b_2 m\left(c'^2_2 - c'^2_1\right)}$$

$$\Phi = \left[1 - \frac{D}{2}(\gamma - 1)\right] e.$$

In order to ensure the non-negativity of d_1 and d_2, c'_1 and c'_2 need to satisfy $c'^2_1 \le D(\gamma - 1)e \le c'^2_2$. However, c'_1 and c'_2 are not completely determined. In practice, we choose c'_1 and c'_2 as close as possible from each other.

Now, the equilibrium distribution is completely determined. When the mean velocity is zero, we have $\rho_1 = \rho$, $\rho_2 = \rho_3 = 0$, therefore, $d_{\nu k} = 0$ for $k = 2$ and 3. In a standard LB model of two particle velocity levels [15], the equilibrium distribution can be written as

$$f^{\mathrm{eq}}_{j\nu} = d_\nu \left\{ 1 + \frac{D}{c^2_\nu} \mathbf{c}_{j\nu} \cdot \mathbf{v} + \frac{D(D+2)}{2c^4_\nu} \left[\mathbf{c}_{j\nu}\mathbf{c}_{j\nu} : \mathbf{vv} - \frac{c^2_\nu}{D} v^2 \right] \right\}.$$

When the mean velocity is zero, this equation becomes

$$f_{jv}^{\mathrm{eq}} = d_v$$

which is the same as Eq. (20). This means that the present model agrees with the standard LB model when the mean velocity is zero.

Considering the relations (15), (16), (17), (26), and (27), we derive the continuity, momentum, and energy equations from Eq. (21),

$$\frac{\partial \rho}{\partial t} + \operatorname{div}(\rho \mathbf{v}) = \operatorname{div}(\mathbf{B}_0) \tag{30}$$

$$\frac{\partial \rho \mathbf{v}}{\partial t} + \operatorname{div}(\rho \mathbf{v}\mathbf{v}) + \nabla p = \operatorname{div}\{\mu[\nabla \mathbf{v} + (\nabla \mathbf{v})^{\mathrm{T}} - (\gamma - 1)\operatorname{div} \mathbf{v}\mathbf{I}] + \mathbf{B}_1\} \tag{31}$$

$$\begin{aligned}\frac{\partial \rho E}{\partial t} + \operatorname{div}(p\mathbf{v} + \rho E \mathbf{v}) = {} & \operatorname{div}\{\mu \mathbf{v} \cdot [\nabla \mathbf{v} + (\nabla \mathbf{v})^{\mathrm{T}} - (\gamma - 1)\operatorname{div} \mathbf{v}\mathbf{I}]\} \\ & + \operatorname{div}\{\nabla A + \nabla(\mu \Phi) - \gamma e \nabla \mu + \mathbf{B}_2\},\end{aligned} \tag{32}$$

where

$$\begin{aligned}
\mu &= \epsilon T \left(\tau - \frac{1}{2}\right) \sum_v m b_v d_v \frac{1}{D} c_v'^2 \\
\mathbf{B}_0 &= \epsilon T \left(\tau - \frac{1}{2}\right) \operatorname{div} \sum_{k,v} m b_v d_{vk} \mathbf{v}_k' \mathbf{v}_k' \\
\mathbf{B}_1 &= \epsilon T \left(\tau - \frac{1}{2}\right) \operatorname{div} \sum_{k,v} m b_v d_{vk} \mathbf{v}\mathbf{v}_k' \mathbf{v}_k' \\
\mathbf{B}_2 &= \epsilon T \left(\tau - \frac{1}{2}\right) \operatorname{div} \sum_{k,v} m b_v d_{vk} \left[\frac{1}{2}\left(v^2 + c_v'^2\right) + \Phi\right] \mathbf{v}_k' \mathbf{v}_k' \\
A &= \epsilon T \left(\tau - \frac{1}{2}\right) \sum_v m b_v d_v \frac{1}{2D} c_v'^4.
\end{aligned} \tag{33}$$

ϵT is the time step; μ is the viscosity. In Eq. (32) the first term and the second term of the right-hand side correspond respectively to the dissipation and the heat conduction. $\mathbf{B}_0$, $\mathbf{B}_1$, and $\mathbf{B}_2$ can be regarded as discretion error. Then, Eqs. (30), (31), and (32) become Navier–Stokes equations. The influences of the fluctuating velocities $\mathbf{v}_k'$ are included in terms $\mathbf{B}_0$, $\mathbf{B}_1$, and $\mathbf{B}_2$ which are of second order of $\mathbf{v}_k'$. Figure 1 shows that $|\mathbf{v}_k'| \le l/\Delta t$, where l is the unit length of the lattice and Δt is the unit time. From Eqs. (24), (26), and (28) we know that when one of the three $|\mathbf{v}_k'|$ takes the maximum $l/\Delta t$ for example, $|\mathbf{v}_{k'}'| = l/\Delta t$, we have $d_{vk'} = 0$. Consequently, $\mathbf{B}_0$, $\mathbf{B}_1$, and $\mathbf{B}_2$ are still small.

When $\mathbf{v}$ is small, $|\mathbf{v}| < \frac{1}{2} l/\Delta t$, for example, one of $\mathbf{v}_k$ is a zero vector (see Fig. 1). Supposing $\mathbf{v}_1 = \mathbf{0}$ without losing generality, we have $\mathbf{v}_1' = -\mathbf{v}$. ρ_2 and ρ_3, solved from Eq. (26), can be written as $\rho_k = \mathbf{a}_k \cdot \mathbf{v}$, $k = 2, 3$, where $\mathbf{a}_k$ are constant vectors determined by $\mathbf{v}_2$ and $\mathbf{v}_3$. In this case, $\mathbf{B}_0$ and $\mathbf{B}_2$ are of order $\mathbf{v}$ and $\mathbf{B}_1$ is of order $\mathbf{v}\mathbf{v}$.

In Ref. [14], $\mathbf{B}_0$, $\mathbf{B}_1$, and $\mathbf{B}_2$ were removed from Eqs. (30), (31), and (32) by modifying the collision invariant $\boldsymbol{\eta}$, while the computation increased about 1/3.

C. *Asymptotic properties.* In the discrete kinetic theory of gases [18] and lattice gas [3], there exists a local H theorem which ensures the stability or asymptotic stability of the models [19–21]. In the LB method we do not have the H theorem. However, due to the simple collision operator of BKG type, we can still analyze the stability of a LB model.

The Boltzmann equation (7) can be written as

$$f(\mathbf{x}+\mathbf{r}\Delta t, \mathbf{r}, \boldsymbol{\xi}, \zeta, t+\Delta t) = f_c(\mathbf{x}, \mathbf{r}, \boldsymbol{\xi}, \zeta, t) \tag{34}$$

$$f_c(\mathbf{x}, \mathbf{r}, \boldsymbol{\xi}, \zeta, t) = f(\mathbf{x}, \mathbf{r}, \boldsymbol{\xi}, \zeta, t) + \Omega(\mathbf{x}, \mathbf{r}, \boldsymbol{\xi}, \zeta, t), \tag{35}$$

where Ω defined by Eq. (8) is a function of f and f^{eq}, the equilibrium distribution defined above. The evolution of $f(\mathbf{x}, \mathbf{r}, \boldsymbol{\xi}, \zeta, t)$ with time consists of two steps: local collision (35) and displacement (34). Considering Eq. (13), we have

$$\sum_{\mathbf{r}\in S} \int_{\mathcal{D}} \boldsymbol{\eta} f_c(\mathbf{x}, \mathbf{r}, \boldsymbol{\xi}, \zeta, t)\, d\boldsymbol{\xi}\, d\zeta = \sum_{\mathbf{r}\in S} \int_{\mathcal{D}} \boldsymbol{\eta} f(\mathbf{x}, \mathbf{r}, \boldsymbol{\xi}, \zeta, t)\, d\boldsymbol{\xi}\, d\zeta. \tag{36}$$

The collision step changes the distribution function f by the amount proportional to the departure of f from the equilibrium distribution f^{eq} under the condition (36). The tendency to the equilibrium distribution can be expected. Especially when $\tau = 1$ the collision operator (35) becomes $f_c(\mathbf{x}, \mathbf{r}, \boldsymbol{\xi}, \zeta, t) = f^{\mathrm{eq}}(\mathbf{x}, \mathbf{r}, \boldsymbol{\xi}, \zeta, t)$.

We can make a rigorous analysis in homogeneous cases. Suppose $f(\mathbf{x}, \mathbf{r}, \boldsymbol{\xi}, \zeta, t)$ is homogeneous at initial time $t = 0$, i.e., $f(\mathbf{x}, \mathbf{r}, \boldsymbol{\xi}, \zeta, 0)$ is independent of $\mathbf{x}$; the lattice is periodic. From the Boltzmann equation (7), $f(\mathbf{x}, \mathbf{r}, \boldsymbol{\xi}, \zeta, t)$ keeps being homogeneous all the time, therefore, the macroscopic variables defined by Eqs. (1), (2), and (3) are always homogeneous and constant. Being completely determined by the macroscopic variables, $f^{\mathrm{eq}}(\mathbf{x}, \mathbf{r}, \boldsymbol{\xi}, \zeta, t)$ is also always homogeneous and constant, i.e., $f^{\mathrm{eq}}(\mathbf{x}, \mathbf{r}, \boldsymbol{\xi}, \zeta, t) = f^{\mathrm{eq}}(\mathbf{x}, \mathbf{r}, \boldsymbol{\xi}, \zeta, 0)$. Equation (7) can be written as

$$f_{n+1}(\mathbf{r}, \boldsymbol{\xi}, \zeta) = \frac{1}{\tau} f_0^{\mathrm{eq}}(\mathbf{r}, \boldsymbol{\xi}, \zeta) + \left(1 - \frac{1}{\tau}\right) f_n(\mathbf{r}, \boldsymbol{\xi}, \zeta), \qquad \forall \mathbf{r} \in S, \boldsymbol{\xi} \in \mathcal{D}_1, \zeta \in \mathcal{D}_0, \tag{37}$$

where $f_n(\mathbf{r}, \boldsymbol{\xi}, \zeta) = f(\mathbf{x}, \mathbf{r}, \boldsymbol{\xi}, \zeta, n\Delta t)$, $f_0^{\mathrm{eq}}(\mathbf{r}, \boldsymbol{\xi}, \zeta)$ is the equilibrium distribution corresponding to the macroscopic variables at initial time. One can see that the equilibrium distribution $f_0^{\mathrm{eq}}(\mathbf{r}, \boldsymbol{\xi}, \zeta)$ is a fix point of Eq. (37). By recurrence of Eq. (37), $f_{n+1}(\mathbf{r}, \boldsymbol{\xi}, \zeta)$ can be calculated

$$\begin{aligned} f_{n+1}(\mathbf{r}, \boldsymbol{\xi}, \zeta) &= \frac{1}{\tau} \sum_{i=0}^{n} \left(1 - \frac{1}{\tau}\right)^i f_0^{\mathrm{eq}}(\mathbf{r}, \boldsymbol{\xi}, \zeta) + \left(1 - \frac{1}{\tau}\right)^{n+1} f_0(\mathbf{r}, \boldsymbol{\xi}, \zeta) \\ &= \left[1 - \left(\frac{1}{\tau}\right)^{n+1}\right] f_0^{\mathrm{eq}}(\mathbf{r}, \boldsymbol{\xi}, \zeta) + \left(1 - \frac{1}{\tau}\right)^{n+1} f_0(\mathbf{r}, \boldsymbol{\xi}, \zeta) \end{aligned} \tag{38}$$

from which we have

$$\lim_{n\to\infty} f_{n+1}(\mathbf{r}, \boldsymbol{\xi}, \zeta) = f_0^{\mathrm{eq}}(\mathbf{r}, \boldsymbol{\xi}, \zeta), \qquad \text{if } \tau > 1/2.$$

At initial time $f_0(\mathbf{r}, \boldsymbol{\xi}, \zeta)$ may be different from the equilibrium distribution $f_0^{\mathrm{eq}}(\mathbf{r}, \boldsymbol{\xi}, \zeta)$ but $f_n(\mathbf{r}, \boldsymbol{\xi}, \zeta)$ tends to the equilibrium distribution if $\tau > 1/2$. Therefore, in the homogeneous case, the equilibrium distribution $f_0^{\mathrm{eq}}(\mathbf{r}, \boldsymbol{\xi}, \zeta)$ is an asymptotically stable fix point if $\tau > 1/2$.

III. NUMERICAL SIMULATIONS

Because the discrete migrating velocity set S contains all $\mathbf{c}_{jvk}$ that vary from node to node and from time to time, S is quite large. Moreover, $\boldsymbol{\xi} \in \mathcal{D}_1$ and $\zeta \in \mathcal{D}_0$ can vary continuously; therefore the Boltzmann equation (7) defined for all $\mathbf{r} \in S$, $\boldsymbol{\xi} \in \mathcal{D}_1$, and $\zeta \in \mathcal{D}_0$ is generally hard to solve. Fortunately, when $\tau = 1$ it is simplified

$$f(\mathbf{x} + \mathbf{r}\Delta t, \mathbf{r}, \boldsymbol{\xi}, \zeta, t + \Delta t) = f^{\mathrm{eq}}(\mathbf{x}, \mathbf{r}, \boldsymbol{\xi}, \zeta, t). \tag{39}$$

Since $f^{\mathrm{eq}}(\mathbf{x}, \mathbf{r}, \boldsymbol{\xi}, \zeta, t)$ depends only on fluid density, velocity, and internal energy, the particle distribution f at $t + \Delta t$ is also determined by them, independent of the particle distribution f at time t. In fact, during the numerical simulations, what we care about are the mass, momentum, and energy transported by the particles, and there is no need to store the particle distribution f. In this way, the need of computer memory and computation time is considerably reduced. Due to the fact that $f^{\mathrm{eq}}(\mathbf{x}, \mathbf{r}, \boldsymbol{\xi}, \zeta, t) = 0$ for $\mathbf{r} \neq \mathbf{c}_{jvk}$, the mass, momentum, and energy transported by a particle from $\mathbf{x}$ to $\mathbf{x} + \mathbf{c}_{jvk}\Delta t$ are the components of the vector

$$\int_{\mathcal{D}} \boldsymbol{\eta} f^{\mathrm{eq}}(\mathbf{x}, \mathbf{c}_{jvk}, \boldsymbol{\xi}, \zeta, t)\, d\boldsymbol{\xi}\, d\zeta = \boldsymbol{\eta}'_{jv} d_{vk}. \tag{40}$$

In the simulations we need only to calculate $\boldsymbol{\eta}'_{jv} d_{vk}$.

If we regard the viscous terms and diffusion terms of the right-hand sides of Eqs. (31) and (32) as the discretion error, Eqs. (30), (31), and (32) become inviscid Euler system. In fact, the viscosity and diffusivity are of order $(\tau - \frac{1}{2})l^2/\Delta t$, where l is the unit length of the lattice and Δt, is the unit time.

Although the theory in the previous section is valid for $\tau > 1/2$, τ has to be 1 for practical simulation in this model. τ appears only in the viscous terms and diffusion terms. Indeed, when solving N-S equations by this model, we lose the freedom of choosing the viscosity and diffusivity by τ, yet we can choose them by other parameters [14]. When we solve Euler equations, the viscous terms and diffusion terms are considered as the discretion error, in this case, the condition $\tau = 1$ does not provoke inconveniences.

In Ref. [12] we simulated the Sod shock-tube problem and two-dimensional shock reflection. The numerical results agree well with the exact solutions. In the following, we simulate three more complex flows with strong shocks under the condition $\tau = 1$ and $\gamma = 1.4$: the forward-facing step, double Mach reflection, and Mach 5.09 diffraction shock tests.

EXAMPLE 1. The forward-facing step test is carried out on a 360×140 hexagonal lattice. The computational domain is 3 : 1. Because of the high speed of the flow, in order to ensure that the constant condition is properly set on the left boundary of the computational domain, at the left of the entrance we add several additional rows of nodes upstream. The constant condition $(\rho, p, u, v) = (1.0, 0.25/1.4, 1.5, 0.)$ is imposed on theses additional nodes. The corresponding Mach number is 3.0. The mirror reflection boundary condition (i.e., slip wall

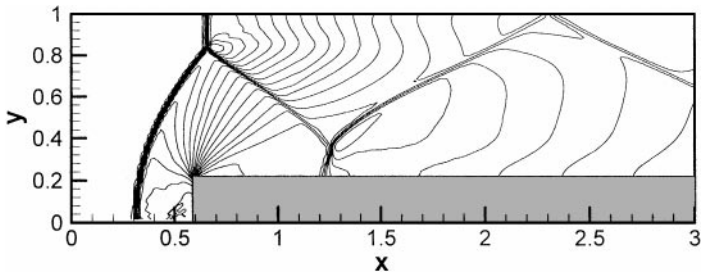

FIG. 2. Density distribution for Mach 3 forward-facing step test on lattice 360×140.

condition) is imposed on the solid walls. The numerical results are presented in Figs. 2–4 for density, pressure, and entropy contours at $t = 1000$th iteration. The shapes and positions of the shocks agree with the those of Refs. [8, 23].

EXAMPLE 2. The next numerical example is a double Mach reflection of a strong shock test [22] calculated on 360×140 hexagonal lattice. The computational domain is $3:1$. The problem is set up by driving a shock down a tube which contains a wedge as shown in Fig. 5. The fluid in front of the shock has zero velocity, and the shock Mach number is equal to 10. The solution to this problem is self-similar, with a function of $(x,\ y,\ t)$ only in the combination $(x/t,\ y/t)$. The density, pressure, and entropy contours at $t = 200$th iteration are shown in Figs. 6–8. Complex features, such as oblique shocks and triple points, are well captured, in good agreement with results obtained by upwind method [22].

EXAMPLE 3. The last numerical example is a strong shock of Mach number 5.09 diffracting around a corner. The computation domain is 1×1, divided into 140×160 cells. Figures 9–11 show the density, pressure, and entropy contours at $t = 140$th iteration. Here again, the shapes and positions of the shocks agree with those of Xu [8]. However, the shocks are not as fine as Xu's. The reason is that our solution is the solution of N-S equations (30), (31), and (32).

Since we store only the mass, momentum, and energy, not the particle distribution function f at each node, the present model consumes less computer memory than traditional models. Although we treat as three times particles ($k = 1, 2, 3$) as traditional LB models, the computation time is almost the same as that of traditional LB models. The reason is that the calculation of the equilibrium distribution is turned to be the calculation of d_{vk} which is independent of j (see Eq. (40)). The simulations were carried out on Pentium II 266 PC. One time step needs 3.4 seconds on 360×140 hexagonal lattice, i.e., about 6.7×10^{-5} seconds per node. The total time is proportional to the total number of nodes.

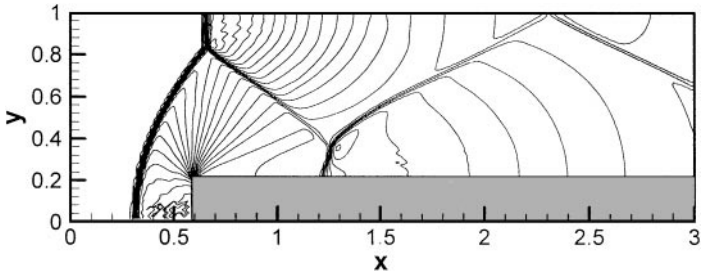

FIG. 3. Pressure distribution for Mach 3 forward-facing step test on lattice 360×140.

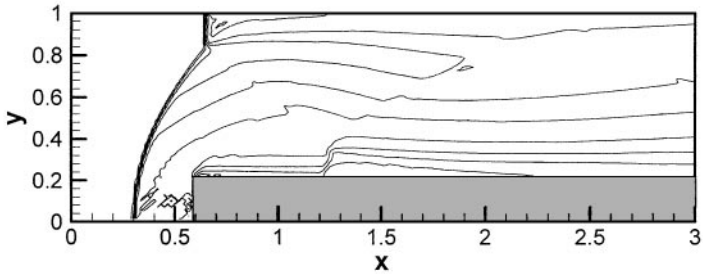

FIG. 4. Entropy distribution for Mach 3 forward-facing step test on lattice 360 × 140.

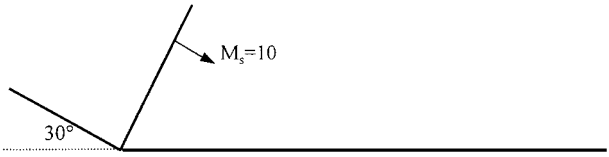

FIG. 5. Initial condition for Mach 10 reflection shock problem.

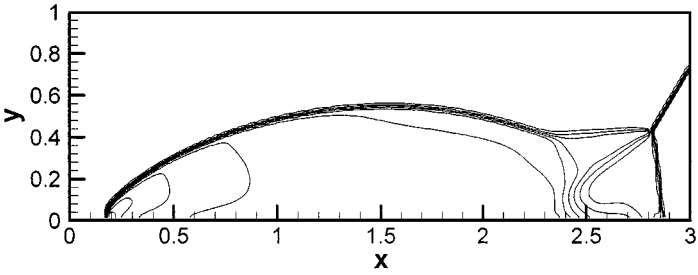

FIG. 6. Density distribution for Mach 10 reflection shock on lattice 360 × 140.

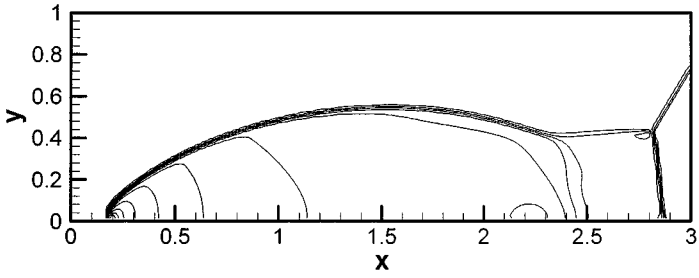

FIG. 7. Pressure distribution for Mach 10 reflection shock on lattice 360 × 140.

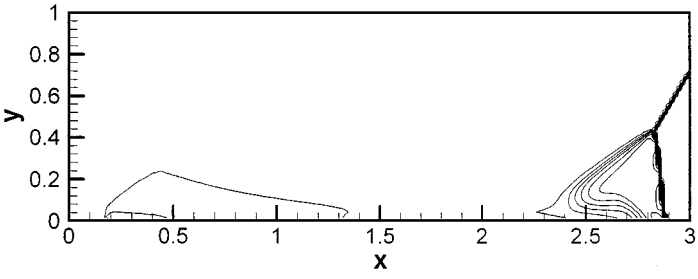

FIG. 8. Entropy distribution for Mach 10 reflection shock on lattice 360 × 140.

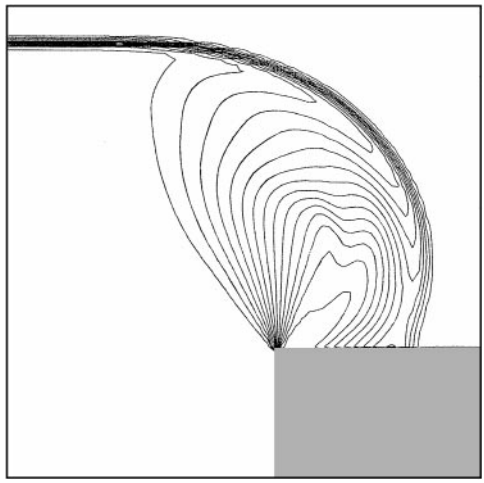

FIG. 9. Density distribution for Mach 5.09 diffraction shock test.

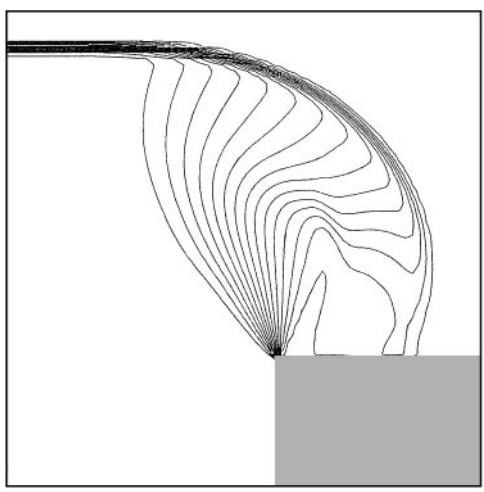

FIG. 10. Pressure distribution for Mach 5.09 diffraction shock test.

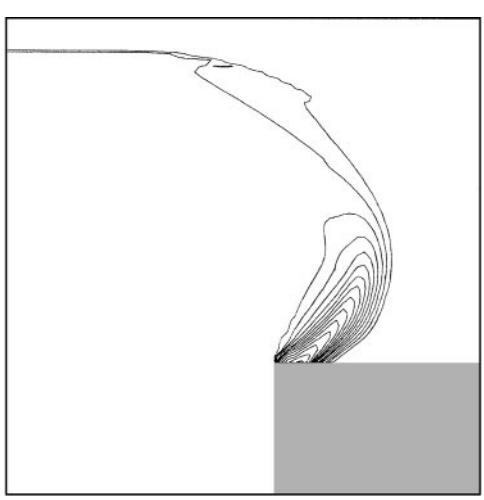

FIG. 11. Entropy distribution for Mach 5.09 diffraction shock test.

IV. CONCLUSION

We present an adaptive LB model to simulate compressible flow and in particular the propagation of strong shock waves. The particle-velocity set is so large that the mean flow may have a high velocity. The support set of the equilibrium-distribution function is quite small and varies with the mean velocity and internal energy. Therefore, the model not only can handle flows over a wide range of Mach numbers and capture shock jumps, but also is simple and applicable. The BGK Boltzmann equation is the basic equation. The Navier–Stokes equations are derived by the Chapman–Enskog method. We have performed the forward-facing step test, the double Mach reflection test, and a strong shock of Mach number 5.09 diffracting around a corner. The shocks are well captured and agree with the results of the other computational methods. These simulations show that the present LB model is effective for flows with strong shocks. It is as efficient as standard LB models and consumes less computer memory. The total computation time is proportional to the total number of nodes. The scheme can be easily adapted to parallel computers. In the numerical simulations we have taken the advantage of the condition $\tau = 1$; otherwise, the simulations would need enormous computer memory and time.

ACKNOWLEDGMENTS

The author thanks D. Bernardin, O. Sero-Guillaume, S. Chen, H. Chen, D. Doolen, and S. Succi for helpful discussions. This work was supported by the National Natural Science Foundation of China (Grants 19672030 and 19972037) and by Scientific Research Foundation for Returned Overseas Chinese Scholars, State Education Ministry.

REFERENCES

1. S. Chen and G. D. Doolen, Lattice Boltzmann method for fluid flows, *Ann. Rev. Fluid Mech.* **30**, 329 (1998).
2. U. Frisch, B. Hasslacher, and Y. Pomeau, Lattice gas automata for the Navier–Stokes equation, *Phys. Rev. Lett.* **56**, 1505 (1986).
3. U. Frisch, D. d'Humières, B. Hasslacher, P. Lallemand, Y. Pomeau, and J. P. Rivet, Lattice gas hydrodynamics in two and three dimensions, *Complex Syst.* **1**, 649 (1987).
4. H. Chen, S. Chen, and W. Matthaeus, Recovery of the Navier–Stokes equation using a lattice-gas Boltzmann method, *Phys. Rev. A* **45**(8), R5339 (1992).
5. Y. H. Qian, D. d'Humières, and P. Lallemand, Lattice BGK models for Navier–Stokes equation, *Europhys. Lett.* **17**(6), 479 (1992).
6. R. Benzi, S. Succi, and M. Vergassola, Lattice Boltzmann equation: Theory and applications, *Phys. Rep.* **222**(3), 145 (1992).
7. K. Xu, A new class of gas-kinetic relaxation schemes for the compressible Euler equations, *J. Statist. Phys.* **81**(1/2), 147 (1995).
8. K. Xu, L. Martinelli, and A. Jameson, Gas-kinetic finite volume methods, flux-vector splitting, and artificial diffusion, *J. Comput. Phys.* **120**, 48 (1995).
9. B. T. Nadiga, An Euler solver based on locally adaptive discrete velocities, *J. Statist. Phys.* **81**(1/2), 129 (1995).
10. F. J. Alexander, H. Chen, and G. D. Doolen, Lattice Boltzmann model for compressible fluids, *Phys. Rev. A* **46**(4), 1967 (1992).
11. S. X. Hu, G. W. Yan, and W. P. Shi, Lattice Boltzmann model for compressible perfect gas, *Acta Mech. Sinica* **13**(3), 314 (1997).
12. C. H. Sun, Lattice-Boltzmann models for high speed flows, *Phys. Rev. E* **58**(6), 7283 (1998).

13. C. H. Sun, Thermal lattice Boltzmann model for compressible fluid, *Chin. Phys. Lett.* **17**(3), 209 (2000).
14. C. H. Sun, Adaptive lattice Boltzmann model for compressible flows: Viscous and conductive properties, *Phys. Rev. E* **61**(3), 2645 (2000).
15. C. H. Sun, Z. Xu, B. Wang, and M. Shen, Lattice Boltzmann models for heat transfer, *Comm. Nonlinear Sci. Numer. Simulation* **2**(4), 212 (1997).
16. D. Bernardin and O. Sero-Guillaume, Lattice gas mixtures models for masse diffusion, *Eur. J. Mech. B* **9**(1), 21 (1990)
17. D. Bernardin, O. Sero-Guillaume, and C. H. Sun, Multi-species 2D lattice gas with energy levels: Diffusive properties, *Phys. D* **47**, 169 (1991).
18. R. Gatignol, *Théorie cinétique des gaz à répartition discrète de vitesse*, in Lecture Notes in Phys. (Springer-Verlag, Berlin, 1975), Vol. 36.
19. C. H. Sun, *Contribution à l'étude de la thermodynamique des gaz sur réseaux*, Ph.D. Dissertation, LEMTA L'Institut National Polytechnique de Lorrain, Nancy, France, 1993.
20. C. H. Sun and J. J. Shi, Study of the stability of the homogeneous Boltzmann equation for lattice gases, *Chinese J. Numer. Math. Appl.* **22**(2), 1 (2000).
21. D. Bernardin and O. Sero-Guillaume, Exact stability results in stochastic lattice gas cellular automata, *J. Statist. Phys.* **81**(1/2), 406 (1995).
22. P. Colella, Multidimensional upwind methods for hyperbolic conservation laws, *J. Comput. Phys.* **87**, 171 (1990).
23. P. Woodward and P. Colella, The numerical simulation of two-dimensional fluid flow with strong shocks, *J. Comput. Phys.* **54**, 115 (1984).